



Quantitative Efficacy and Fate of Mesenchymal Stromal Cells Targeted to Cardiac Sites by Radiofrequency Catheter Ablation

Cell Transplantation
Volume 29: 1–12
© The Author(s) 2020
Article reuse guidelines:
sagepub.com/journals-permissions
DOI: 10.1177/0963689720914236
journals.sagepub.com/home/ccl


Rizwan Malik¹, Fabrice F. Darche^{1,2}, Rasmus Rivinius^{1,2},
Anja Seckinger³, Ulf Krause^{3,4}, Michael Koenen^{1,5},
Dierk Thomas^{1,2}, Hugo A. Katus^{1,2}, and Patrick A. Schweizer^{1,2} 

Abstract

Engraftment and functional integration of stem cells or stem cell-derived cells within cardiac tissue is an important prerequisite for cell replacement therapy aiming at the treatment of heart disease. Recently, a novel intravenous approach for application of mesenchymal stromal cells (MSCs) to cardiac sites has been established using radiofrequency catheter ablation (RFCA)-guided targeting, bypassing the need for open chest surgery or direct myocardial cell injection. However, little is known about the quantitative efficacy and longevity of this strategy. We performed selective power-controlled RFCA with eight ablation pulses (30 W, 60 s each) to induce heat-mediated lesions at the right atrial appendices (RAAs) of pigs. Different concentrations of human bone marrow-derived MSCs (10^5 to 1.6×10^6 cells/kg bodyweight) labeled with superparamagnetic iron oxide (SPIO) particles were infused intravenously in nine pigs one d after RFCA treatment and hearts were explanted 8 d later to quantify the number of engrafted cells. Prussian blue staining revealed high numbers of SPIO-labeled cells in areas surrounding the RFCA-induced lesions. Cell numbers were evaluated by quantitative real-time polymerase chain reaction using specific primers for human MSCs (hMSCs), which indicated that up to 10^6 hMSCs, corresponding to $\sim 3.9\%$ of the systemically applied human cells, engrafted within the RAAs of RFCA-treated pigs. Of note, infused hMSCs were observed in nontargeted organs, as well, but appeared at very low concentrations. To assess long-term deposition of MSCs, RAAs of three pigs were analyzed after 6 months, which revealed few persisting hMSCs at targeted sites. RFCA-mediated targeting of MSCs provides a novel minimal invasive strategy for cardiac stem cell engraftment. Qualitative and quantitative results of our large animal experiments indicate an efficient guidance of MSCs to selected cardiac regions, although only few cells remained at targeted sites 6 mo after cell transplantation.

Keywords

mesenchymal stromal cells, catheter ablation, homing, cell therapy

Introduction

Strategies for stem cell application in cardiology are multiple, including cell therapy approaches to treat ischemic, structural, or degenerative cardiac diseases^{1–3}. Besides the choice of a suitable cell type aiming at cardiac transdifferentiation and functional integration, the development of effective and gentle cell delivery methods is of high priority⁴. Recently, in addition to thoracotomy and open chest cell injection, transendocardial, intracoronary, and intravenous (IV) approaches for cell application have been established and beneficial effects using these techniques have been shown by several independent groups^{4–6}. However, problems to track and quantify the number of viable cells that

¹ Department of Cardiology, Medical University Hospital Heidelberg, Heidelberg, Germany

² DZHK (German Centre for Cardiovascular Research), Partner Site Heidelberg/Mannheim, University of Heidelberg, Heidelberg, Germany

³ Department of Hematology, Oncology and Rheumatology, Medical University Hospital Heidelberg, Heidelberg, Germany

⁴ Institute for Transfusion Medicine and Cellular Therapy, University Hospital Muenster, Domagstrasse, Muenster, Germany

⁵ Department of Molecular Neurobiology, Max-Planck-Institute for Medical Research, Jahnstrasse, Heidelberg, Germany

Submitted: December 31, 2019. Revised: February 7, 2020. Accepted: February 28, 2020.

Corresponding Author:

Patrick A. Schweizer, MD, Department of Cardiology, University of Heidelberg, INF 410, D-69120 Heidelberg, Germany.
Email: patrick.schweizer@med.uni-heidelberg.de



integrated into the myocardium made it difficult to assess efficacy of these approaches^{7,8}. Like ischemic myocardium, which is capable to elicit homing effects on multiple stem cell sources, radiofrequency catheter ablation (RFCA) has been used to induce local stem cell delivery to specified regions of the atrium after IV cell application^{9,10}. In search for a novel approach to overcome electrical pacemakers, several groups were able to create a biological pacemaker in large animal models based on plasmid-mediated overexpression of pacemaker genes in mesenchymal stromal cells (MSCs)^{11,12}. However, these studies were limited by the necessity of open thoracotomy and direct cell injections to guide transduced stem cells to a selected myocardial region. The novel approach using RFCA-guided homing^{9,10} may allow for targeting MSCs close to the sinoatrial node to reestablish pacemaker function, avoiding open chest surgery. However, open questions concerning efficacy of the method, long-term outcome including safety issues such as immune tolerance, oncogenicity, and cell migration to non-targeted organs remain to be addressed.

In the present study, we used RFCA to guide intravenously applied human MSCs (hMSCs) to the right atrium in a pig model. In an effort to quantify the number of migrated cells we established a quantitative real-time polymerase chain reaction (qRT-PCR) approach using highly specific primers for hMSC detection to evaluate the efficacy of the method. Furthermore, we evaluated the hearts 6 mo post hMSC application to investigate targeted and remote organ engraftment.

Materials and Methods

All experiments were carried out in accordance with the *Guide for the Care and Use of Laboratory Animals* published by the US National Institute of Health (NIH publication number 85–23, revised 1996), and with the European Community guidelines for the use of experimental animals as well as all relevant ethical regulations. Protocols were approved by the local regulatory authority (AZ #359185.81/G-128/05 and AZ #359185.81/G-67/11, Regierungspräsidium Karlsruhe, Germany).

Radiofrequency Catheter Ablation

An IV cannula in the ear vein was used for administration of fluids and drugs. Domestic swine (body weight 20 to 25 kg) were sedated with ketamine (100 mg/kg; Roche, Grenzach-Wyhlen, Germany) and midazolam (15 mg/kg, intramuscular; Roche), and anesthetized with disoprivane (1 ml of a 1% solution; Astra Zanecca, Wedel, Germany) and isoflurane (1% to 2%; Baxter, Unterschleissheim, Germany). Lesions in the right auricle were induced by transvenous power-controlled RFCA (Cerablate easy catheter, bipolar, 4 mm tip and HAT 200™ RF generator; Sulzer Osypka GmbH, Grenzach-Wyhlen, Germany). The ablation catheter was introduced via preparation of the right femoral vein and

inserted under fluoroscopic guidance until the tip was located at the wall of the auricle in the right atrium. Each animal obtained eight ablation pulses (30 W/500 kHz, power-controlled mode, each pulse 60 s). Electrocardiographic leads I, II, III, aVR, aVL, and aVF were continuously monitored with a VR12™-recorder (Electronics for Medicine, Pleasantville, NY, USA).

Isolation of hMSCs

MSCs were obtained from bone marrow aspirates from the iliac crest of healthy donors after approval by the local ethical committee (University of Heidelberg ethical committee numbers 042/2000 and 251/2002) as published previously^{9,13–15}. In brief, approximately 10 to 30 ml of bone marrow was collected in a syringe containing 10,000 IU heparin to prevent coagulation. The mononuclear cell fraction was isolated by density gradient centrifugation (Biocoll, Biochrom, Berlin Germany) and plated on tissue culture flasks (Nunc, Thermo Fisher Scientific, Waltham, MA, USA) coated with 10 ng/ml fibronectin (Sigma, Kawasaki, Kanagawa, Japan). Expansion medium consisted of 58% low-glucose Dulbecco's modified Eagle medium (Cambrex, East Rutherford, NJ, USA), 40% MCDB201 (Sigma), 2% fetal calf serum (FCS, Hyclone, Thermo Fisher Scientific), supplemented with 2 mM L-glutamine, 100 U/ml Pen/Strep (Gibco, Eggenstein, Germany), 1% insulin transferrin selenium, 1% linoleic acid bovine serum albumin, 10 nM dexamethasone, 0.1 mM L-ascorbic acid-2-phosphate (all from Sigma), platelet-derived growth factor, and epidermal growth factor (10 ng/ml each, R&D Systems, Minneapolis, MN, USA). At 80% confluency, cells were trypsinized (0.25% trypsin/1 mM ethylenediaminetetraacetic acid [EDTA], Invitrogen, Karlsruhe, Germany), washed with phosphate buffered saline (PBS, Cambrex), and reseeded at a density^{13,14} of 5 to 10,000 cells/cm². To confirm cell identity, flow cytometry as well as in vitro differentiation assays were performed as published previously¹⁵. Antibodies were tested in advance for specificity in vitro. Appropriate controls were performed in all experiments.

Labeling of MSCs

To track MSCs after transplantation, cells were labeled with superparamagnetic iron oxides (SPIOs)¹⁶. In brief, cells were incubated for 18 h in expansion medium containing 25 µg iron (Endorem®, Guerbet GmbH, Villepinte, France) and 0.75 µg poly-L-lysine (Sigma) per ml, respectively. Afterwards, cells were washed three times with PBS, trypsinized and resuspended in PBS containing 1% FCS and 2 mM EDTA at a final concentration of 1×10^7 cells/ml.

MSC Application and Terminal Experiment

For proof of concept using the porcine model, two swine received 5×10^6 hMSCs, each labeled with SPIOs. MSCs

were applied 1 d after RFCA via an IV cannula in the ear vein by 10 ml 0.9% saline to wash the cannula. For quantitative assessment, different numbers (1.0×10^5 to 1.6×10^6 per kg bodyweight [BW]) of hMSCs were applied in nine swine, each receiving a defined number of hMSCs. Two sham experiments were performed, using animals that were only treated by RFCA but received PBS infusion only for control purpose. For evaluation of long-term deposition, three additional animals were treated with 5×10^5 MSCs/kg BW each, 1 d after RFCA of the RAAs, and transplant recipients were followed up for 6 mo (please refer to supplemental Table 1 for overview). Final experiments were performed under deep propofol anesthesia 1 and 24 wk after MSC application using 4 mEq KCl IV to arrest the heart. Hearts were then exposed through a midsternotomy and washed in 0.9% NaCl. After optical inspection, right auricles were excised, cut into two pieces and frozen on isopenthan/dry ice or fixed in 3% formaldehyde at 4°C for at least 72 h. For PCR investigation of local stem cell distribution, samples from isopenthan frozen sections were dissected in defined intervals from the central lesion using a specified die cutter (sample diameter 2 mm). For calculation of total cell numbers migrated to RAAs, whole RAA sections were frozen on isopenthan/dry ice and analyzed by qRT-PCR.

Histology and Immunohistochemistry

Frozen right appendices were dissected by slices from the basis to the apex using sections of 15 and 30 μm , which were prepared at -15°C to -20°C using a cryotome (Bright Microtome 5030, Huntingdon, England) and stored at -20°C . Prussian blue staining was performed with 15, 30, and 300 μm slices prepared from fixed appendices at 2-mm intervals. Slices were rinsed with PBS (3×2 min), and incubated for 15 min with 1% potassium ferrocyanide (Perl's reagent for Prussian blue staining) in 1% hydrochloric acid. Following several washes with PBS, sections were counterstained with hematoxylin and eosin following standard protocols and analyzed using a Stemi SV6 loupe microscope (Zeiss, Jena, Germany). Immunofluorescence analysis was performed in a two-step staining protocol. Sections were rinsed with PBS, fixed in 1% formaldehyde for 30 min at room temperature, and incubated in blocking solution (0.1 M glycine, 2% bovine serum albumin, and 2% horse serum in PBS) for 2 to 3 h. MSCs were detected by overnight staining at 4°C using the primary anti-CD44 antibody (rat anti-CD44 immunoglobulin G [IgG], EMD Biosciences, San Diego, CA, USA) diluted 1:200 in blocking solution. After washes with PBS (3×2 min), sections were incubated for 3 h at 4°C with a secondary antibody Alexa Fluor[®] 568 goat anti-rat IgG antibody (Invitrogen), rinsed with PBS (3×2 min) and counterstained with DAPI. Sections were mounted in Citifluor[™] glycerol/PBS solution (Agar Scientific, Stansted, England) and analyzed by light and fluorescence microscopy using a Zeiss Axioplan

2 fluorescence microscope (Zeiss) with an Intas LC110C camera (Intas, Göttingen, Germany).

Isolation of RNA and cDNA Synthesis

For isolation of total RNA the tissues were homogenized and prepared using a polytron homogenizer and the TRIzol-Reagent (Invitrogen) method, according to the manufacturer's instructions. Total RNA was reverse transcribed in 100 μl containing $5 \times$ First Strand Buffer (Invitrogen), 30 U RNAGuard (GE Healthcare Europe, Freiburg, Germany), 1.1 mM dNTP (Invitrogen, Carlsbad, CA, USA), 11.3 mM DTT (Invitrogen), 5 μg Pd(N)₆ random hexamer primers (GE Healthcare), and 1,000 U Superscript II Reverse Transcriptase (Invitrogen). Fifteen micrograms of total RNA was added to the mixture after being incubated for 5 min at 68°C, put 2 min on ice and incubated for 1 h at 37°C.

Quantitative real-time polymerase chain reaction

Quantification was performed using an ABS 7500 RT-PCR system and 96-well optical detection plates (Thermo Fisher, Waltham, MA, USA). Wells were loaded to a total volume of 25 μl consisting of 10 to 50 ng cDNA, and $1 \times$ TaqMan Universal Master Mix and TaqMan primers and probes (TaqMan Gene Expression Assays, Thermo Fisher). We designed PCR primers and a TaqMan probe, hybridizing specifically to sequences encoding human glycerinaldehyde-3-phosphate-dehydrogenase (hGAPDH) transcripts (forward: AATCCCATCACCATCTTCCA, reverse: TGGACTC CACGACGTACTCA), yielding negligible signals of reporter dye fluorescence in samples containing exclusively porcine myocardial transcripts, while predesigned TaqMan probes and primers (TaqMan Gene Expression Assays, Thermo Fisher) were used to detect porcine GAPDH (pGAPDH; Ss03374854_g1). Probes were labeled with the fluorescent reporter dye 6-carboxyfluorescein (Thermo Fisher) at the 5'-end and with the nonfluorescent quencher at the 3'-end. Cycling conditions comprised an initial denaturing step at 95°C (10 min), and 45 cycles with 95°C (15 s) and 60°C (40 s). Data were analyzed using the threshold cycle (C_T) relative quantification method^{17–19}. All PCRs were performed in triplicate, and the data are expressed as an average of the triplicates.

Data Analysis

The $\Delta\Delta C_T$ method¹⁷ was used for data analysis, where the C_T value of a target transcript is expressed as a relative change between the two experimental conditions. We calculated target gene expression relative to that of the house-keeping gene GAPDH, which was shown to be expressed relatively stable throughout the pig's cardiac development, between different cardiac tissues and in cardiomyocytes under various conditions.

Table 1. Mean hMSC signal (hGAPDH/pGAPDH) detected in samples (1 to 5) of the RAA with defined distance from the RFCA lesion.

Sample	1.0×10^5 hMSCs/kg BW	2.3×10^5 hMSCs/kg BW	6.8×10^5 hMSCs/kg BW	1.1×10^6 hMSCs/kg BW	1.2×10^6 hMSCs/kg BW	1.6×10^6 hMSCs/kg BW
1 (hGAPDH/pGAPDH)	$0.04 \times 10^{-4} \pm 0.01 \times 10^{-4}$	$0.12 \times 10^{-4} \pm 0.05 \times 10^{-4}$	$0.09 \times 10^{-4} \pm 0.03 \times 10^{-4}$	$0.18 \times 10^{-4} \pm 0.4 \times 10^{-4}$	$0.25 \times 10^{-4} \pm 0.1 \times 10^{-4}$	$0.68 \times 10^{-4} \pm 0.2 \times 10^{-4}$
2 (hGAPDH/pGAPDH)	$1.62 \times 10^{-4} \pm 0.5 \times 10^{-4}$	$6.88 \times 10^{-4} \pm 1 \times 10^{-4}$	$33 \times 10^{-4} \pm 5 \times 10^{-4}$	$44 \times 10^{-4} \pm 10 \times 10^{-4}$	$62 \times 10^{-4} \pm 6.5 \times 10^{-4}$	$79.5 \times 10^{-4} \pm 4 \times 10^{-4}$
3 (hGAPDH/pGAPDH)	$2.31 \times 10^{-4} \pm 0.6 \times 10^{-4}$	$2.4 \times 10^{-4} \pm 0.4 \times 10^{-4}$	$13.4 \times 10^{-4} \pm 6.5 \times 10^{-4}$	$3.81 \times 10^{-4} \pm 1.2 \times 10^{-4}$	$1.7 \times 10^{-4} \pm 0.6 \times 10^{-4}$	$6.1 \times 10^{-4} \pm 3.7 \times 10^{-4}$
4 (hGAPDH/pGAPDH)	$0.01 \times 10^{-4} \pm 0.007 \times 10^{-4}$	$0.18 \times 10^{-4} \pm 0.08 \times 10^{-4}$	$4.93 \times 10^{-4} \pm 1.3 \times 10^{-4}$	$0.14 \times 10^{-4} \pm 0.05 \times 10^{-4}$	$1.2 \times 10^{-4} \pm 0.3 \times 10^{-4}$	$2.7 \times 10^{-4} \pm 1.2 \times 10^{-4}$
5 (hGAPDH/pGAPDH)	$0.41 \times 10^{-4} \pm 0.1 \times 10^{-4}$	$0.12 \times 10^{-5} \pm 0.5 \times 10^{-6}$	$0.96 \times 10^{-4} \pm 0.2 \times 10^{-4}$	$0.1 \times 10^{-5} \pm 0.3 \times 10^{-6}$	$0.15 \times 10^{-5} \pm 0.7 \times 10^{-6}$	$0.02 \times 10^{-5} \pm 0.1 \times 10^{-6}$

BW: body weight; hGAPDH: human glyceraldehyde-3-phosphate-dehydrogenase; hMSCs: human mesenchymal stem cells; pGAPDH: porcine glyceraldehyde-3-phosphate-dehydrogenase; RFCA: radio-frequency catheter ablation.

Statistical Analysis

The average of the relative transcript levels of each group of samples was characterized by calculating the arithmetic means as well as the standard deviation of the individual reactions. We used Microsoft Excel 2010 (Microsoft Corporation, Redmond, WA, USA) and SPSS 18 (IBM SPSS Statistics 18, Somers, NY, USA) for statistical analysis. Data were further evaluated with Fisher's exact test and matched with the Mann-Whitney *U*-test because of the small number of pigs for the experiments ($n < 6$).

Results

Qualitative Evidence for RFCA-Mediated Targeting of hMSCs in a Pig Model

RFCA-induced lesions were shown to target systemically applied MSCs to the right atrial appendix (RAA) of dogs without the need for open chest surgery or direct cell injection^{9,10}. We set out to transfer this approach to a swine model using xenogeneic transfer of hMSCs to swine atrial myocardium. To this end we performed selective power-controlled RFCA with eight ablation pulses (30 W, 60 s each) to induce heat-mediated lesions at the RAAs of two pigs (Fig. 1A, B). The next day, 5×10^6 hMSCs, labeled with SPIOs, were infused intravenously in each animal. Eight days later, hearts were explanted and the RAA was cryosectioned. Adjacent to the necrotic lesion, myocardial structure was destroyed and interstitially rearranged (Fig. 2A–E). Intercellular spaces were filled with small cells heavily loaded with Prussian blue-positive particles thought to cause the bluish appearance of the border zone, indicating that SPIO-labeled MSCs had engrafted within the lesion border zone (Fig. 2D, E). Counterstaining with anti-CD44, a typical surface marker of MSCs, displayed a close morphological correlation of Prussian blue-stained cells and CD44-positive mesenchymal structures (Fig. 3A–D). These observations pointed to an abundant engraftment of systemically applied xenogeneic hMSCs to the lesion border zones, confirming the results of our previously published dog model using allogeneic canine MSCs⁹.

Mapping the Distribution of hMSC Engraftment by RT-PCR

To address the efficacy of the method, we aimed to quantify the distribution and peak concentration of engrafted hMSCs within the border zone adjacent to the RFCA lesion, but also the average content of hMSCs in the whole RAA of the treated pigs. To this end, we designed PCR primers and a TaqMan probe, hybridizing specifically to sequences encoding hGAPDH transcripts, yielding negligible signals of reporter dye fluorescence in samples containing exclusively porcine myocardial transcripts, while producing clear and reproducible signals in myocardial samples containing $\geq 0.001\%$ human cDNA (supplemental Figure S1). Thus,

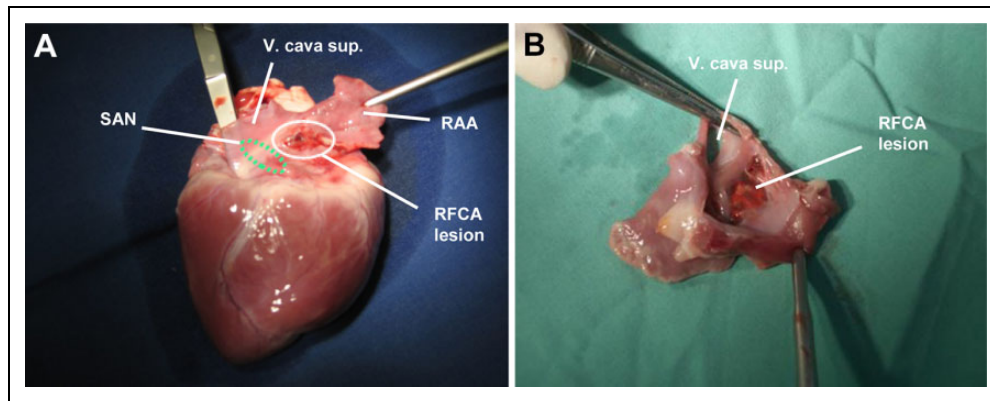


Figure 1. Macroscopic view of the heart of a domestic pig treated by RFCA on the basis of the RAA. (A) Lesion at the RAA 7 d after radiofrequency catheter ablation. (B) Endocardial aspect of an isolated RAA with transmural RFCA lesion. RAA: right atrial appendix; RFCA: radiofrequency catheter ablation.

we established an RT-PCR assay that utilized the relation between human and pGAPDH levels to evaluate the proportion of engrafted xenogeneic hMSCs within the porcine tissue.

Quantitative Analysis of hMSCs Within the Border Zone of the RFCA Lesion. Based on the distinct gradient of Prussian blue-stained cells adjacent to the central necrotic lesion, we asked whether different transcript levels of hGAPDH derived from migrated hMSCs could be detected, as well. Starting from the necrotic lesion five tissue samples were dissected from the frozen RAA in 3 to 4 mm steps (Fig. 4). While the samples from the inner part of the necrotic lesion showed negligible hGAPDH signals, the border zone (sample 2) yielded the highest hGAPDH levels, declining toward the periphery (Fig. 4, Table 1). This distribution was evident in RFCA-treated RAAs of all animals irrespective of the number of hMSCs that were administered. However, the hGAPDH/pGAPDH ratios detected were strictly dependent on the number of the systemically applied hMSCs, showing peak hGAPDH/pGAPDH ratios of $79.5 \times 10^{-4} \pm 4 \times 10^{-4}$ at the border zone (sample 2) of animals that had received the maximum cell number (1.6×10^6 hMSCs/kg BW) (Fig. 5A, Table 1).

Total Yield of hMSCs Within the RAA. Regarding the number of hMSCs totally migrated to the RAA, we performed RNA isolation of the whole RAA using the TRIzol method and the consecutive cDNA reverse transcriptase to examine the total yield of hGAPDH transcripts within the RAA. Concentration of engrafted hMSCs was evaluated through hGAPDH/pGAPDH ratios using the designed, highly species-specific primers. As expected, we observed increasing hGAPDH/pGAPDH ratios within the RAAs, rising in parallel with the number of infused hMSCs up to a ratio of 2.6×10^{-4} at 1.1×10^6 hMSCs/kg BW (Fig. 5B). Interestingly, IV application of higher numbers of hMSCs did not yield further increase of hGAPDH/pGAPDH ratios in the

RAAs (Fig. 5B), suggesting that migration of hMSCs to the myocardium may reach steady-state saturation and cannot be further augmented by raising the number of infused cells.

Based on the calibration curves of hGAPDH transcripts derived from defined numbers of hMSCs (supplemental Figure S1) we calculated the number of hMSCs engrafted within the whole RAA. Assuming the maximum hGAPDH/pGAPDH ratio of 2.6×10^{-4} (supplemental Table S1), up to $3.9 \pm 1.4\%$ of hMSCs that were applied intravenously 1 wk prior were detectable within the RAA, corresponding to a total number of $\sim 10^6$ engrafted hMSCs. In control animals, however, which received PBS injection only, no hGAPDH signal was detected in the RAAs.

Evidence for hMSCs at Nontargeted Organs

To evaluate distribution and quantity of hMSCs at nontargeted organs we carefully examined lung, liver, spleen, and kidney samples of animals treated with SPIO-labeled hMSCs. Even in animals that received highest hMSC numbers in our experimental setting (1.1 to 1.6×10^6 cells/kg BW) Prussian-blue-positive cells were detected only sporadically within lung tissue (Fig. 6A, B), while spleen and kidney samples did not provide evidence of nontargeted hMSC spread. With regard to liver tissue it is important to note that Prussian-blue cells are ubiquitously detectable, which is well explained by liver Kupffer cells, known to be Prussian-blue positive, yielding similar effects in control animals only treated with PBS (not shown). Using our RT-PCR-based quantification assay for hMSCs, we observed negligible hGAPDH signals, with hGAPDH/pGAPDH $<10^{-5}$ in samples of all nontargeted organs investigated, indicating an aberrant yield of hMSCs beyond the detection level of the assay.

Long-Term Deposition of hMSCs at the RAAs

We next asked whether engrafted hMSCs persist at their position adjacent to RFCA lesions throughout a period of 6

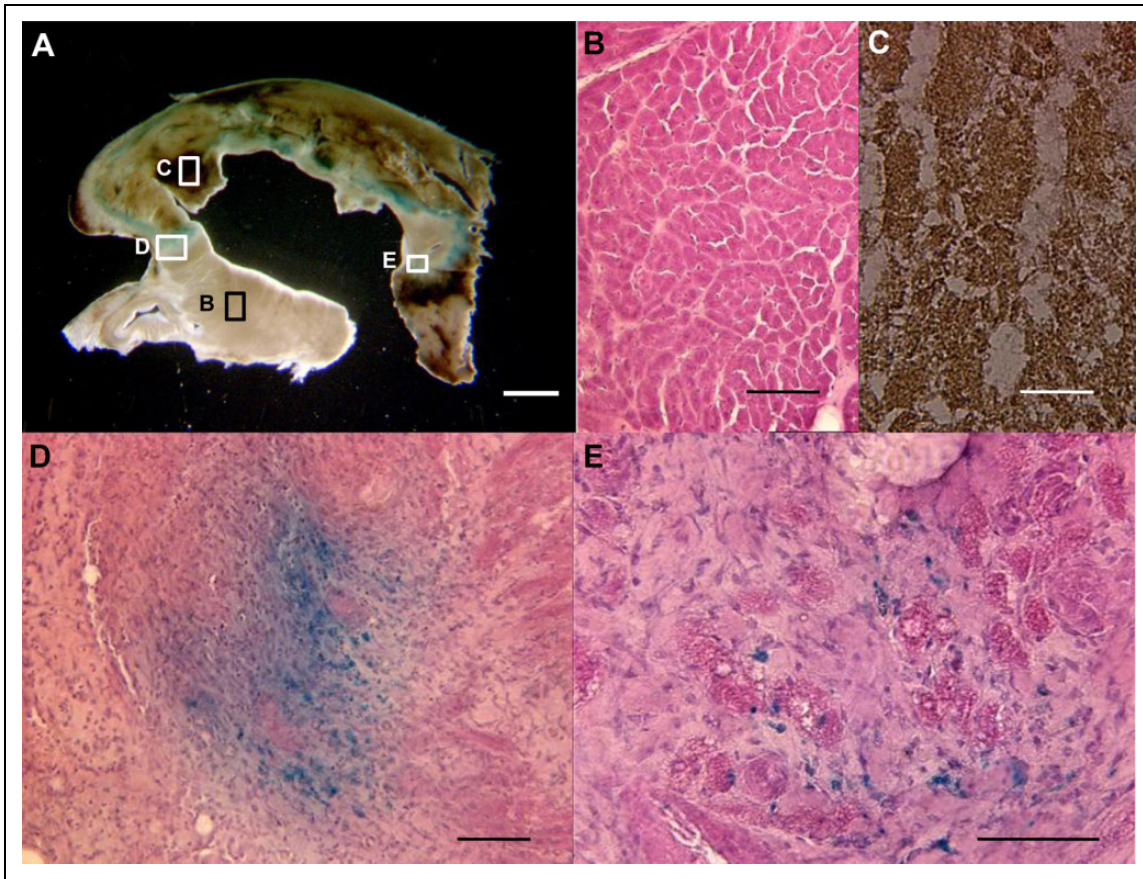


Figure 2. Microscopic analysis of Prussian blue-stained lesion of the RAA. (A) Loupe-microscopic view of a 300 μm section of the RAA showing necrotic tissue caused by RFCA, a bluish-stained border zone, and unaffected intact myocardium. Scale bar = 5 mm. (B) Unaffected myocardium. Scale bar = 100 μm . (C) Lesion with necrotic tissue. Scale bar = 100 μm . (D–E) Migration of Prussian blue-positive cells into the border zone and along intercellular spaces, indicating engraftment of SPIO-labeled MSC toward the affected myocardium. Scale bar = 100 μm .

MSC: mesenchymal stem cell; RAA: right atrial appendix; RFCA: radiofrequency catheter ablation.

mo post IV injection. To address this question three animals were treated with 5×10^5 hMSCs/kg BW each, 1 d after RFCA of the RAAs according to our customized protocol, with one animal receiving SPIO-labeled hMSCs. Transplant recipients were followed up for 6 mo, and animals were sacrificed thereafter. Hearts were harvested and prepared for histological and molecular evaluation. It required in-depth histological examination to recognize scarred areas of the RAAs corresponding to RFCA lesions after 6 mo. Qualitative assessment was undertaken in the animal that had received SPIO-labeled MSCs using Prussian blue staining, which unmasked few small punctual accumulations of bluish deposits in the vicinity of the scarred regions (Fig. 6C, D). Molecular evaluation was undertaken using qPCR to detect xenograft hMSC transplants in the two additional animals. hGAPDH signals derived from whole RAA preparations were tiny and hGAPDH/pGAPDH ratios were below 10^{-5} (2.37×10^{-6} and 4.61×10^{-6} , respectively). In addition, we carefully examined nontargeted organs lung, liver, spleen, and kidney by Prussian blue staining and qPCR for

hGAPDH signals in these animals, respectively, and did not find evidence for measurable aberrant deposition of hMSCs.

Thus, >90% of hGAPDH/pGAPDH levels, which are related to hMSC engraftment within the RAAs 1 wk post application, were nondetectable 6 mo later, most likely due to cellular redistribution and dilution or death/rejection of transplanted cells. Of note, all hearts were free from macrophage or lymphocyte infiltrations, neoplasm-like cell accumulations, or tumors.

Discussion

We here report the quantification and evaluation of long-term fate of hMSCs guided to a specified cardiac site by local RFCA. An important issue, crucial to any cell therapy, is sufficient cell engraftment within the target region. To address this critical point we have developed a qPCR-based assay for quantifying the levels of hMSCs transplanted to the porcine myocardium. Using this assay we could show that hMSCs that were systemically applied to pigs, which

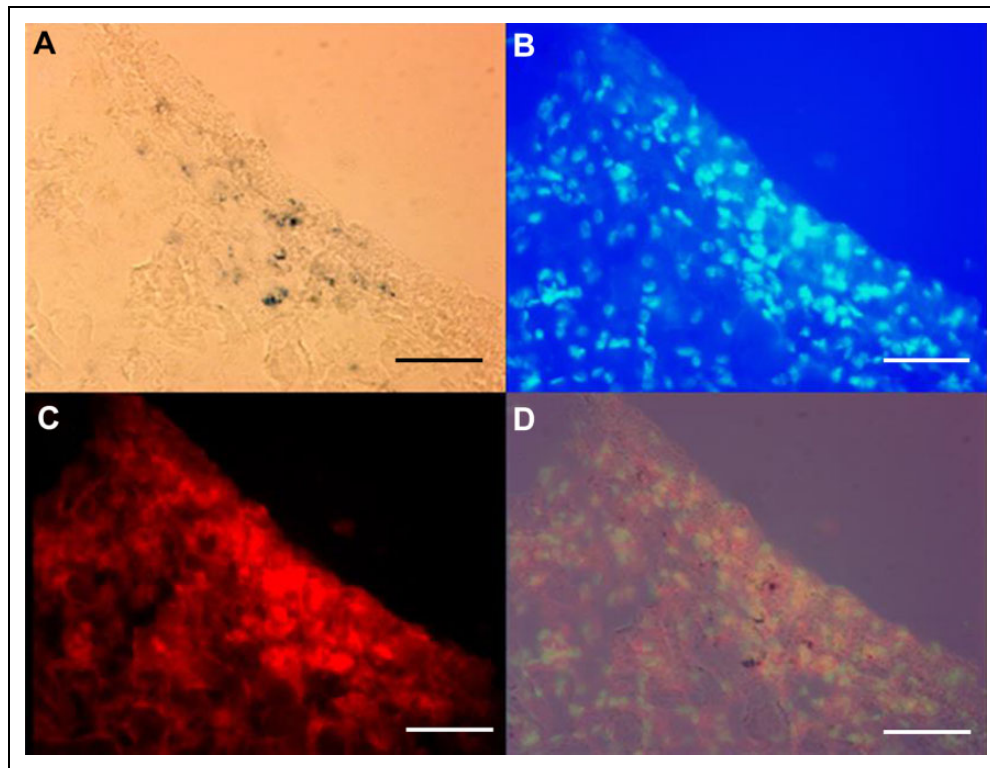


Figure 3. Histological characterization of Prussian blue-positive regions. (A) Prussian blue-stained cryosection (15 μm) of the right atrial appendix border zone counterstained with 4',6-diamidino-2-phenylindole (B), immunostained with antibodies directed against the mesenchymal cell surface marker CD44 (red) (C). (D) Overlay of A, B, and C. Scale bar (A–D) = 100 μm .

underwent RFCA of the RAAs the day prior, could be detected within the border zone of the lesions in a dose-dependent fashion, 1 wk after cell application. Furthermore, our data suggest that the total number of cells engrafted to the RAA may reach steady-state saturation and cannot be further augmented by raising the number of infused cells.

Usually evaluation of cell transplantation efficiency within an organ is extrapolated from histological sections using microscopic strategies²⁰ or by tracking of labeled cells using *in vivo* imaging techniques^{21,22}. Accuracy of histological methods depends on the quality of sectioning, and possible bias comprises different thickness of sections, variations of cell diameters, and local accumulation of cells²³. These concerns also apply to cell tracking by *in vivo* imaging, which requires high-resolution cell detection to distinguish transplanted cells from background noise⁷. Recent works have revealed shortcomings of *in vivo* magnetic resonance imaging, as cell tracking techniques often do not clearly distinguish between living cells and extracellular nanoparticle remnants⁸.

Using a molecular assay that is based on the detection of xenogeneic human GAPDH messenger RNA by qPCR, we took advantage from the unique and species-specific design of TaqMan probes employed to evaluate the copy number of target template in transplanted cells. This strategy detects the

molecular footprint of transplanted cells and as such is highly sensitive, precise, and fast. Furthermore, evidence of mRNA presumes that it derives from viable cells, providing evidence for the integrity of engrafted MSCs.

Our results indicate that a relatively high proportion of cells temporarily engraft to cardiac injury border zones. This is in agreement with previous data from studies investigating stem cell homing after myocardial infarction, which could show that applied MSCs were detected adjacent to myocardial necrosis and may contribute to reverse remodeling^{2,5,8,24,25}. However, the observation that cells, which engrafted at cardiac sites of injury, have the tendency to reallocate or undergo local apoptosis was described previously in studies using *in vivo* models of myocardial infarction^{8,26}, and was observed in the present study using RFCA-induced cardiac lesions, as well. Using a TUNEL assay-based approach Ma et al.⁸ could show that allogeneic MSCs, which were transplanted successfully after myocardial infarction in a rat model, underwent apoptosis gradually over time, and almost disappeared after several weeks. Their results indicated that the microenvironment of damaged cardiac tissue, infiltrated by macrophages and inflammatory cells, activates apoptotic pathways in the transplanted MSCs⁸.

Based on these data, it is questionable whether permanent cellular deposition at cardiac target sites, qualifying for cell replacement therapy, can be achieved using this approach, i.e.,

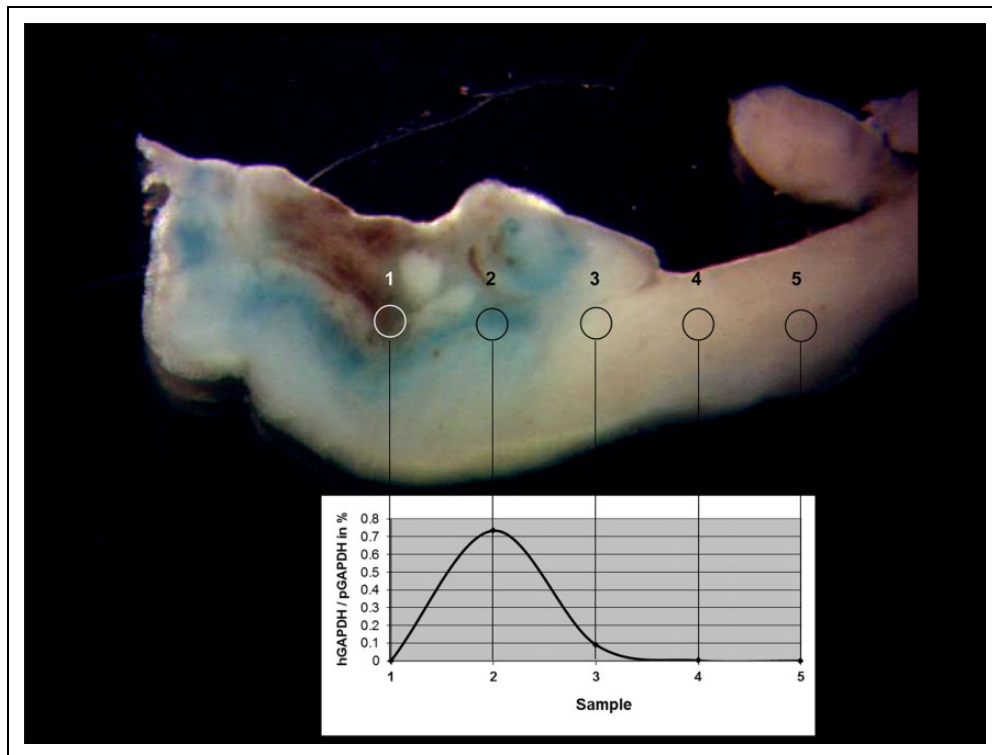


Figure 4. Loupe-microscopic view of a right atrial appendix section indicating a central radiofrequency catheter ablation lesion adjacent to a border zone with local accumulation of Prussian blue-positive hMSCs. Samples in defined distance to the lesion were dissected for quantification of hMSC engraftment using quantitative polymerase chain reaction (hGAPDH/pGAPDH signal ratios), as indicated. hGAPDH: human glyceraldehyde-3-phosphate-dehydrogenase; hMSC: human mesenchymal stem cell; pGAPDH: porcine glyceraldehyde-3-phosphate-dehydrogenase.

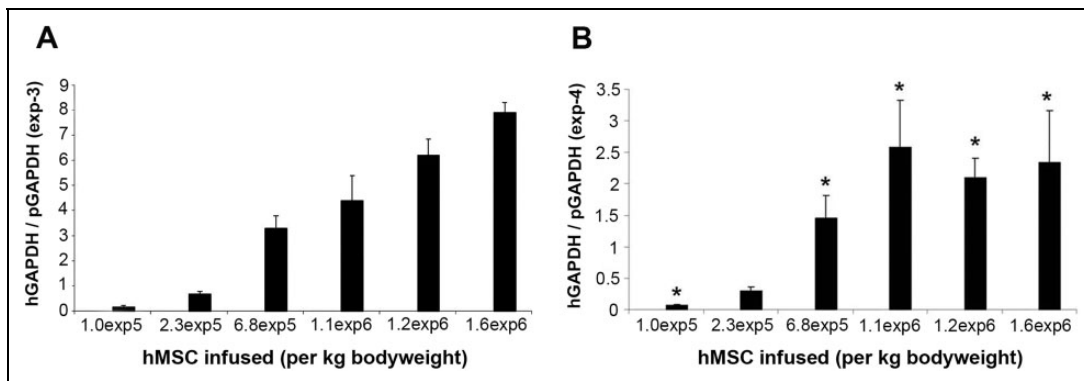


Figure 5. Quantitative evaluation of the engrafted hMSCs by quantitative polymerase chain reaction–based analysis of local hGAPDH signals. (A) Presentation of the hGAPDH/pGAPDH ratios at the border zones (sample 2) adjacent to the lesion in relation to the number of systemically applied hMSCs ($n = 3$ to 6). (B) Average hGAPDH/pGAPDH ratios of the whole right atrial appendix ($n = 3$ to 6 experimental replications) in relation to the number of systemically applied hMSCs. * $P < 0.05$ related to hGAPDH/pGAPDH in animals that received 2.3×10^5 MSCs/kg bodyweight. Data are expressed as mean \pm standard error of the mean. hGAPDH: human glyceraldehyde-3-phosphate-dehydrogenase; hMSC: human mesenchymal stem cell; pGAPDH: porcine glyceraldehyde-3-phosphate-dehydrogenase.

in the case of a cellular biological pacemaker, transplanted cells might exert only temporal pacemaker function and may cease functioning after a relatively short period of time. Nevertheless, the strategy could be of interest to bridge cardiac

pacemaking for a limited period in situations like cardiac infection with the necessity to extract leads of an electronic pacemaker. However, accumulation of systemically applied cells at a selected cardiac region for a limited time frame may appear

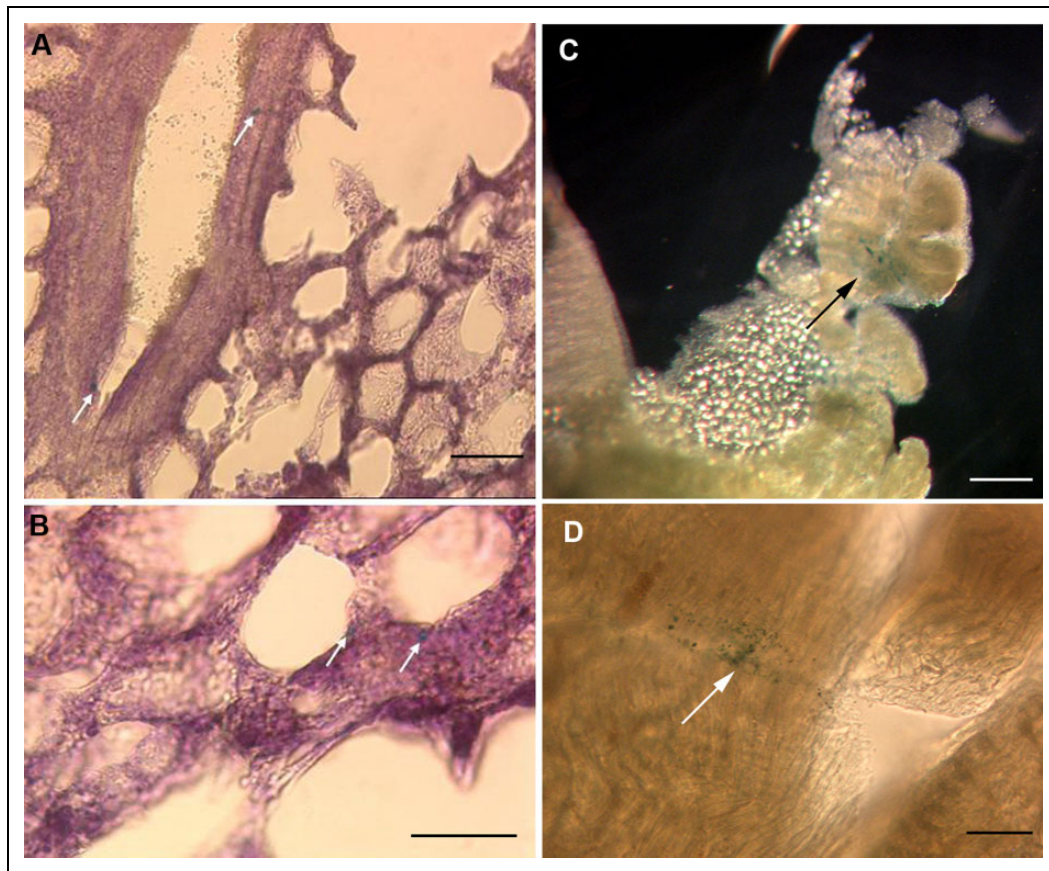


Figure 6. Aberrant and long-term RAA deposition of hMSCs. (A, B) Paraffin slice (30 μm) of the lung stained by hematoxylin and eosin and Prussian blue staining. Singular Prussian blue-positive cells are indicated by arrow, next to the bronchus (A) or to alveoli (B), and suggestive for aberrant engraftment of systemically applied hMSCs. Scale bar: A = 200 μm , B = 100 μm . (C, D) Macroscopic view of RAA sections derived from a pig, treated by RFCA and superparamagnetic iron oxide-labeled hMSC application 6 mo prior. Localized, small punctual accumulations of bluish deposits in the vicinity of the scarred regions are indicated by arrow. Scale bars (C, D) = 100 μm . RAA: right atrial appendix; hMSC: human mesenchymal stem cell.

tempting for alternative approaches, as well. Remarkably, in this context, 1 wk after systemic application, up to 3.9% of cells, which correspond to a total number of $\sim 10^6$ presumably viable MSCs, were guided to the RAAs. These cells may be utilized for therapeutic purpose, i.e., delivery of paracrine mediators, shuttle for gene therapy, or pharmacological substances. In this context, novel adjuvant strategies using cell-based approaches after RFCA of cardiac arrhythmias may be of interest. For example, after catheter ablation of cardiac arrhythmias electrical instability is typically increased for several weeks, originating from the site of ablation, not necessarily indicating worse outcome of the procedure (so-called early recurrence or blanking period)²⁷. Short-term pro-arrhythmic mechanisms are most likely caused by local inflammatory reactions post ablation. MSCs are known to electrically integrate within the myocardium via gap junctions¹¹ and by this transport membrane potential to neighbor cardiomyocytes. Forced in vitro expression of ionic currents in MSCs that counteract spontaneous electrical activity by hyperpolarizing membrane potential, like inward rectifying K(+) current (mediated by Kir2.1

channels), and subsequent delivery of MSCs to RFCA sites in vivo may effectively reduce the pro-arrhythmic risk post ablation. The antiarrhythmic effect of such a hybrid gene/cell therapeutic approach has been reported previously by transplantation of embryonic stem cell-derived cardiomyocytes overexpressing Kir2.1 to mouse hearts post myocardial infarction²⁸. Furthermore, MSCs have been shown to attenuate inflammation in acute myocardial infarction²⁹ and may exert similar effects at cardiac ablation sites, counteracting early arrhythmia recurrence from local inflammatory reactions. Noteworthy, we did not observe any signs of malignancy or tumor formation in the animals that received transplanted MSCs, not in the heart or in the other organs that were macroscopically and microscopically examined, given the small number of pigs that underwent long-term follow-up.

Limitations

The quantification approach for transplanted cells used in this study is based on xenogeneic cell transfer. Although

MSCs were reported to comprise a reduced immunoreactivity even in xenogeneic applications^{11,30,31}, it cannot be ruled out that the marked reduction of cells after 6 mo of follow-up is caused by immunorejection and consecutive death of transplanted cells. Immunoprivilege of MSC is most likely mediated by masking of cellular surface antigens, through cellular secretion of prostaglandins and other immune modulators^{31,32}. Noteworthy, transplanted MSCs may differentiate into more mature cell types and it is questionable whether they will maintain their immunoprivileged status over time³³. Thus, it might be important that transplanted hMSCs remain in an undifferentiated state and additional studies are required to determine whether maturation and differentiation may cause loss of immunoprotection and may promote rejection. Alternatively, use of autologous MSCs could prevent immunorejection and cell death³³, although additional mechanisms that result in reduction of local cell numbers, like re-allocation of transplanted cells, may remain. Only a limited number of pigs were subjected to this large animal study, which was primarily designed as a pilot trial, implying some restrictions with respect to the statistical strength of the data.

Conclusion

Considerable numbers of systemically applied MSCs can be temporarily directed to a cardiac target site using RFCA, and may be utilized for specified therapeutic purpose. By providing a method of quantifying the amount of engrafted cells within the target region, our qPCR-based assay serves as a novel and precise tool to evaluate the efficacy of cell engraftment applications to specified organs.

Acknowledgment

We thank Simone Bauer for the excellent technical work.

Ethical Approval

Ethical approval to report this study was obtained from the University of Heidelberg ethical committee (approval numbers 042/2000 and 251/2002). Animal experiments were approved by the local regulatory authority (AZ #359185.81/G-128/05 and AZ #359185.81/G-67/11, Regierungspräsidium Karlsruhe, Germany).

Statement of Human and Animal Rights

All procedures in this study were conducted in accordance with the local ethical committee (University of Heidelberg ethical committee) and study protocols were approved by the University of Heidelberg ethical committee (approval numbers 042/2000 and 251/2002). Animal experiments were approved by the local regulatory authority (AZ #359185.81/G-128/05 and AZ #359185.81/G-67/11, Regierungspräsidium Karlsruhe, Germany).

All experiments were carried out in concordance with the Declaration of Helsinki. Animal experiments were carried out in accordance with the Guide for the Care and Use of Laboratory Animals published by the US National Institute of Health (NIH publication number 85–23, revised 1996), and with the European

Community guidelines for the use of experimental animals as well as all relevant ethical regulations.

Statement of Informed Consent

Written informed consent was obtained from the patients for their anonymized information to be published in this article.


Declaration of Conflicting Interests

The author(s) declared no potential conflicts of interest with respect to the research, authorship, and/or publication of this article.

Funding

The author(s) disclosed receipt of the following financial support for the research, authorship, and/or publication of this article: This research was funded in parts by grants from the Max-Planck-Society (TANDEM project to Michael Koenen and Patrick A. Schweizer), from the Ministry of Science, Research and the Arts Baden-Wuerttemberg (Sonderlinie Medizin to Dierk Thomas), from the German Heart Foundation (Kaltenbach scholarship to Fabrice F. Darche), from the Heidelberg Medical Faculty (*Physician Scientist-Programm* to Fabrice F. Darche and Rasmus Rivinius) from the German Cardiac Society (Research Scholarship to Rasmus Rivinius), from the ADUMED Foundation (Research Scholarship to Ulf Krause), and from the German Centre for Cardiovascular Research (DZHK). Patrick A. Schweizer is recipient of the Heidelberg Research Centre for Molecular Medicine (HRCMM) Senior Career Fellowship.

ORCID iD

Patrick A. Schweizer  <https://orcid.org/0000-0002-7212-1202>

Supplemental Material

Supplemental material for this article is available online.

References

1. Menasché P. Cell therapy trials for heart regeneration - lessons learned and future directions. *Nat Rev Cardiol.* 2018;15(11):659–671.
2. Fan M, Huang Y, Chen Z, Xia Y, Chen A, Lu D, Wu Y, Zhang N, Qian J. Efficacy of mesenchymal stem cell therapy in systolic heart failure: a systematic review and meta-analysis. *Stem Cell Res Ther.* 2019;10(1):150.
3. Darche FF, Rivinius R, Köllensperger E, Leimer U, Germann G, Seckinger A, Hose D, Schröter J, Bruehl C, Draguhn A, Gabriel R, et al. Pacemaker cell characteristics of differentiated and HCN4-transduced human mesenchymal stem cells. *Life Sci.* 2019;232:116620.
4. Freyman T, Polin G, Osman H, Crary J, Lu M, Cheng L, Palasis M, Wilensky RL. A quantitative, randomized study evaluating three methods of mesenchymal stem cell delivery following myocardial infarction. *Eur Heart J.* 2006;27(9):1114–1122.
5. Wolf D, Reinhard A, Seckinger A, Katus HA, Kuecherer H, Hansen A. Dose-dependent effects of intravenous allogeneic mesenchymal stem cells in the infarcted porcine heart. *Stem Cells Dev.* 2009;18(2):321–329.

6. Hare JM, Fishman JE, Gerstenblith G, DiFede Velazquez DL, Zambrano JP, Suncion VY, Tracy M, Gherlin E, Johnston PV, Brinker JA, Breton E, et al. Comparison of allogeneic vs autologous bone marrow-derived mesenchymal stem cells delivered by transendocardial injection in patients with ischemic cardiomyopathy: the POSEIDON randomized trial. *JAMA*. 2012;308(22):2369–2379.
7. Frangioni JV, Hajar RJ. In vivo tracking of stem cells for clinical trials in cardiovascular disease. *Circulation* 2004; 110(21):3378–3383.
8. Ma N, Cheng H, Lu M, Liu Q, Chen X, Yin G, Zhu H, Zhang L, Meng X, Tang Y, Zhao S. Magnetic resonance imaging with superparamagnetic iron oxide fails to track the long-term fate of mesenchymal stem cells transplanted into heart. *Sci Rep*. 2015;5:9058.
9. Schweizer PA, Krause U, Becker R, Seckinger A, Bauer A, Hardt C, Eckstein V, Ho AD, Koenen M, Katus HA, Zehelein J. Atrial-radiofrequency catheter ablation mediated targeting of mesenchymal stromal cells. *Stem Cells*. 2007;25(6): 1546–1551.
10. Kim U, Shin DG, Park JS, Kim YJ, Park SI, Moon YM, Jeong KS. Homing of adipose-derived stem cells to radiofrequency catheter ablated canine atrium and differentiation into cardiomyocyte-like cells. *Int J Cardiol*. 2011;146(3):371–338.
11. Plotnikov AN, Shlapakova I, Szabolcs MJ, Danilo P Jr, Lorell BH, Potapova IA, Lu Z, Rosen AB, Mathias RT, Brink PR, Robinson RB, et al. Xenografted adult human mesenchymal stem cells provide a platform for sustained biological pacemaker function in canine heart. *Circulation*. 2007;116(7): 706–713.
12. Lu W, Yaoming N, Boli R, Jun C, Changhai Z, Yang Z, Zhiyuan S. mHCN4 genetically modified canine mesenchymal stem cells provide biological pacemaking function in complete dogs with atrioventricular block. *Pacing Clin Electrophysiol*. 2013;36(9):1138–1149.
13. Niemeyer P, Krause U, Fellenberg J, Kasten P, Seckinger A, Ho AD, Simank HG. Evaluation of mineralized collagen and alpha-tricalcium phosphate as scaffolds for tissue engineering of bone using human mesenchymal stem cells. *Cells Tissues Organs*. 2004;177(2):68–78.
14. Gottschling S, Saffrich R, Seckinger A, Krause U, Horsch K, Miesala K, Ho AD. Human mesenchymal stromal cells regulate initial self-renewing divisions of hematopoietic progenitor cells by a beta1-integrin-dependent mechanism. *Stem Cells*. 2007;25(3):798–806.
15. Wagner W, Wein F, Seckinger A, Frankhauser M, Wirkner U, Krause U, Blake J, Schwager C, Eckstein V, Ansoerge W, Ho AD. Comparative characteristics of mesenchymal stem cells from human bone marrow, adipose tissue, and umbilical cord blood. *Exp Hematol*. 2005;33(11):1402–1416.
16. Arbab AS, Bashaw LA, Miller BR, Jordan EK, Bulte JW, Frank JA. Intracytoplasmic tagging of cells with ferumoxides and transfection agent for cellular magnetic resonance imaging after cell transplantation: methods and techniques. *Transplantation*. 2003;76(7):1123–1130.
17. Livak KJ, Schmittgen TD. Analysis of relative gene expression data using real-time quantitative PCR and the 2(-Delta Delta C(T)) Method. *Methods*. 2001;25(4):402–408.
18. Schweizer PA, Yampolsky P, Malik R, Thomas D, Zehelein J, Katus HA, Koenen M. Transcription profiling of HCN-channel isoforms throughout mouse cardiac development. *Basic Res Cardiol*. 2009;104(6):621–629.
19. Yampolsky P, Koenen M, Mosqueira M, Geschwill P, Nauck S, Witzemberger M, Seyler C, Fink T, Kruska M, Bruehl C, Schwoerer AP, et al. Augmentation of myocardial If dysregulates calcium homeostasis and causes adverse cardiac remodeling. *Nat Commun*. 2019;10(1):3295.
20. Schmuck EG, Koch JM, Centanni JM, Hacker TA, Braun RK, Eldridge M, Hei DJ, Hematti P, Raval AN. Biodistribution and Clearance of Human Mesenchymal Stem Cells by Quantitative Three-Dimensional Cryo-Imaging After Intravenous Infusion in a Rat Lung Injury. *Model Stem Cells Transl Med*. 2016; 5(12):1668–7165.
21. Kraitchman DL, Tatsumi M, Gilson WD, Ishimori T, Kedziorek D, Walczak P, Segars WP, Chen HH, Fritzges D, Izbudak I, Young RG, et al. Dynamic imaging of allogeneic mesenchymal stem cells trafficking to myocardial infarction. *Circulation*. 2005;112(10):1451–61.
22. Schmuck EG, Koch JM, Hacker TA, Hatt CR, Tomkowiak MT, Vigen KK, Hendren N, Leitzke C, Zhao YQ, Li Z, Centanni JM, et al. Intravenous followed by X-ray fused with MRI-guided transendocardial mesenchymal stem cell injection improves contractility reserve in a swine model of myocardial infarction. *J Cardiovasc Transl Res*. 2015;8(7):438–448.
23. McBride C, Gaupp D, Phinney DG. Quantifying levels of transplanted murine and human mesenchymal stem cells in vivo by real-time PCR. *Cytotherapy*. 2003;5(1):7–18.
24. Dash R, Kim PJ, Matsuura Y, Ikeno F, Metzler S, Huang NF, Lyons JK, Nguyen PK, Ge X, Foo CW, McConnell MV, et al. Manganese-enhanced magnetic resonance imaging enables in vivo confirmation of peri-infarct restoration following stem cell therapy in a porcine ischemia-reperfusion model. *J Am Heart Assoc*. 2015;4(7):e002044.
25. Florea V, Rieger AC, DiFede DL, El-Khorazaty J, Natsumeda M, Banerjee MN, Tompkins BA, Khan A, Schulman IH, Landin AM, Mushtaq M, et al. Dose Comparison study of allogeneic mesenchymal stem cells in patients with ischemic cardiomyopathy (The TRIDENT Study). *Circ Res*. 2017; 121(11):1279–1290.
26. Huang Z, Li C, Yang S, Xu J, Shen Y, Xie X, Dai Y, Lu H, Gong H, Sun A, Qian J, et al. Magnetic resonance hypointensive signal primarily originates from extracellular iron particles in the long-term tracking of mesenchymal stem cells transplanted in the infarcted myocardium. *Int J Nanomedicine*. 2015;10:1679–7990.
27. Andrade JG, Khairy P, Verma A, Guerra PG, Dubuc M, Rivard L, Deyell MW, Mondesert B, Thibault B, Talajic M, Roy D, et al. Early recurrence of atrial tachyarrhythmias following radiofrequency catheter ablation of atrial fibrillation. *Pacing Clin Electrophysiol*. 2012;35(1):106–1016.

28. Liao SY, Tse HF, Chan YC, Mei-Chu Yip P, Zhang Y, Liu Y, Li RA. Overexpression of Kir2.1 channel in embryonic stem cell-derived cardiomyocytes attenuates posttransplantation proarrhythmic risk in myocardial infarction. *Heart Rhythm*. 2013;10(2):273–282.
29. Du YY, Zhou SH, Zhou T, Su H, Pan HW, Du WH, Liu B, Liu QM. Immuno-inflammatory regulation effect of mesenchymal stem cell transplantation in a rat model of myocardial infarction. *Cytotherapy*. 2008;10(5):469–478.
30. Di Nicola M, Carlo-Stella C, Magni M, Milanesi M, Longoni PD, Matteucci P, Grisanti S, Gianni AM. Human bone marrow stromal cells suppress T-lymphocyte proliferation induced by cellular or nonspecific mitogenic stimuli. *Blood*. 2002;99(10):3838–3843.
31. Lee RH, Pulin AA, Seo MJ, Kota DJ, Ylostalo J, Larson BL, Semprun-Prieto L, Delafontaine P, Prockop DJ. Intravenous hMSCs improve myocardial infarction in mice because cells embolized in lung are activated to secrete the anti-inflammatory protein TSG-6. *Cell Stem Cell*. 2009;5(1):54–63.
32. Tse WT, Pendleton JD, Beyer WM, Egalka MC, Guinan EC. Suppression of allogeneic T-cell proliferation by human marrow stromal cells: implications in transplantation. *Transplantation*. 2003;75(3):389–97.
33. Huang XP, Sun Z, Miyagi Y, McDonald Kinkaid H, Zhang L, Weisel RD, Li RK. Differentiation of allogeneic mesenchymal stem cells induces immunogenicity and limits their long-term benefits for myocardial repair. *Circulation*. 2010;122(23):2419–2429.